

Squeezed Abrikosov-Josephson Vortex in Atomic-Layer Pb Superconductors Formed on Vicinal Si(111) Substrates


Yudai Sato^{1,*}, Masahiro Haze¹, Ryohei Nemoto,² Wenxuan Qian,³ Shunsuke Yoshizawa⁴,
Takashi Uchihashi^{2,3} and Yukio Hasegawa^{1,†}

¹*The Institute for Solid State Physics, The University of Tokyo, 5-1-5 Kashiwa-no-ha, Kashiwa, 277-8581, Japan*

²*International Center for Materials Nanoarchitectonics (WPI-MANA), National Institute for Materials Science, 1-1 Namiki, Tsukuba, 305-0044, Japan*

³*Graduate School of Science, Hokkaido University, Kita-10 Nishi-8, Kita-ku, Sapporo 060-0810, Japan*

⁴*Research Center for Advanced Measurement and Characterization, National Institute for Materials Science, 1-2-1 Sengen, Tsukuba, 305-0047, Japan*

 (Received 27 April 2022; revised 4 November 2022; accepted 3 February 2023; published 10 March 2023)

Unlike bulk counterparts, two-dimensional (2D) superconductors are sensitive to disorder. Here, we investigated superconductivity of Pb atomic layers formed on vicinal substrates to reveal how surface steps with an interval shorter than the coherence length ξ affect it. Electrical transport showed reduced critical temperature and enhanced critical magnetic field. Scanning tunneling microscopy exhibited vortices elongated along the steps, that is, Abrikosov-Josephson vortices squeezed normal to the steps due to the reduced ξ . These results demonstrate that steps work as disorder and vicinal substrates provide a unique platform to manipulate the degree of disorder on 2D superconductors.

DOI: [10.1103/PhysRevLett.130.106002](https://doi.org/10.1103/PhysRevLett.130.106002)

Two-dimensional (2D) superconductors are sensitive to the presence of disorder because of induced electron localization and phase fluctuation [1–3]. The issue of 2D superconductivity with disorder has been investigated and unique phenomena such as superconductor-insulator transition (SIT) at zero temperature have been explored [4–7]. Recently highly crystalline atomic-layer superconductors have been fabricated in various methods; e.g., by molecular beam epitaxy [4,8–15], mechanical exfoliation [16,17], and the gating through ion liquid [18–21]. On these samples, new schemes of disorder-related phenomena such as the emergence of Bose metal [22] and multifractal phases [13,14] have been reported and discussed extensively.

In the present study, we focus on steps in monolayer superconductors, which work as disorder and behave as a Josephson junction [4,11,12,23]. The role of a single step has been investigated on atomic-layer superconductors by scanning tunneling microscopy (STM) [9–12]. It has been known that the shape of vortex cores trapped at the steps depends on how strongly the step decouples the superconducting states of the neighboring terraces. When the decoupling is weak, round Abrikosov vortex (or Pearl vortex, in more precise description) is pinned at the step. With the intermediate decoupling, trapped vortices are elongated along the step while remaining the superconducting order parameter at the core, which is called a Abrikosov-Josephson vortex (AJV) [24]. In the case of the strongly decoupling step, a further elongated vortex with the order parameter almost the same as that of surrounding

superconducting areas, that is, a Josephson vortex (JV), is formed along the step.

Here we present a new way of introducing disorder into high-quality monolayer superconductors by forming them on vicinal substrates, which have a normal direction slightly tilted from the nominal one, resulting in forming a lot of atomic steps separating (111) terraces. We fabricated the striped incommensurate (SIC) structure, one of the Pb monolayer superconducting phases, on vicinal Si(111) substrates tilted by 1.1° or 0.5° toward the $[\bar{1}\bar{1}2]$ direction from the (111) plane, where steps with the atomic height (0.31 nm) are uniformly distributed without bunching. By just adjusting the miscut angle the step separation can be controlled to make it shorter than the Ginzburg-Landau (GL) coherence length ξ . Details on the sample preparation and experiment are found in Secs. 1-3 in the Supplemental Material [25]. Through the electron transport measurements and STM, we investigated how these high-density steps affect superconducting properties under magnetic fields through the observation of their influences in the transition and vortex shape, and demonstrated their significant roles both macroscopically and microscopically.

First, for the investigation of the superconducting transition, we performed surface electron transport measurements through the SIC layer formed on flat and 1.1° -tilted vicinal substrates (Fig. 1). As is the case of other 2D superconductors, the sheet resistances R at zero magnetic field shown in Figs. 1(a), 1(b) is reduced above T_c due to the thermal fluctuation in the amplitude of the superconducting order parameter. The enhanced conductance

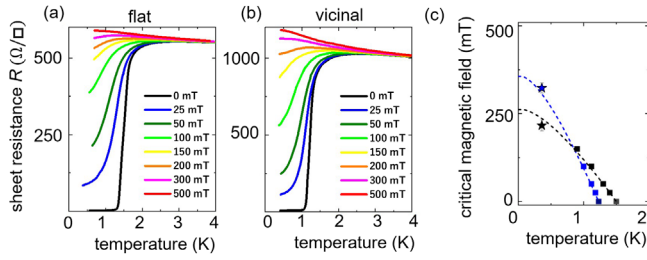


FIG. 1. (a),(b) temperature dependence of sheet resistance measured on the SIC samples formed (a) on a flat and (b) on a 1.1° -tilted vicinal substrates under out-of-plane magnetic fields. (c) temperature dependence of the upper critical magnetic field B_{c2} . Black and blue squares indicate B_{c2} determined by the UD scaling theory (below 150 mT) on the flat and vicinal samples, respectively. The dashed curves are the WHH fitting curves. The stars mark B_{c2} measured by STM at 0.36 K.

above T_c is described by the 2D Aslamazov-Larkin and Maki-Thompson terms [32–34]. We obtained $T_{c,\text{flat}} = 1.51$ K and $T_{c,\text{vicinal}} = 1.21$ K from the fitting with the two terms [See Secs. 3,4 and Figs. S3(b),(c) in the Supplemental Material [25]]. T_c is reduced by the introduction of the steps since the disorder suppresses superconductivity through the Anderson localization and phase fluctuation [5,15,35–37].

Next, we focus on out-of-plane magnetic field dependence of R . Under the magnetic fields in a range of 25 to 100 mT, we found the finite resistance remaining near zero temperature, suggesting the emergence of the quantum metallic state reported on highly crystalline 2D superconductors [18,19,38]. By applying more than 300 mT, R behaves in an insulating manner ($dR/dT < 0$) in the range of 0.4 to 4 K (far above T_c), one of the characteristic features of the magnetic-field driven SIT, intrinsic to 2D superconductors. We applied the Ullah-Dorsey (UD) scaling theory [19] to analyze the data shown in Figs. 1(a),1(b) to evaluate T_c under magnetic fields, that is, temperature dependence of the upper critical field B_{c2} , as shown with squares in Fig. 1(c) (see Sec. 5 of the Supplemental Material [25]). $B_{c2}(T)$ can also be obtained by

Werthamer-Helfand-Hohenberg (WHH) theory [39], as shown in the dashed curves in Fig. 1(c) (see Sec. 6 in the Supplemental Material [25]). We found that $B_{c2,\text{vicinal}}$ is higher than $B_{c2,\text{flat}}$ below 1 K (see Sec. 7 in Supplemental Material [25] for more details). In fact, the WHH curves are consistent with B_{c2} at $T = 0.36$ K measured by STM, as marked with stars in Fig. 1(c), which will be discussed in detail below.

For microscopic understanding of the enhanced B_{c2} , we investigated both flat and vicinal samples using STM at 0.36 K. Figure 2(a) shows an STM image taken on a flat SIC sample and Figs. 2(b)–2(f) are a series of zero bias conductance (ZBC) maps taken on the same area under various magnetic fields. Under the magnetic fields, vortices are formed and the superconductivity is locally broken at their core, resulting in a round high-ZBC area, as shown in the ZBC map taken under 60 mT [Fig. 2(b)]. Raising the magnetic field to 120 mT [Fig. 2(c)] increases the number of vortices. The number of the vortices are consistent with that expected from the amount of applied magnetic field. Under 210 mT [Fig. 2(d)], vortices are hardly visible since most of the areas has high ZBC. At 300 mT [Fig. 2(e)], ZBC is nearly uniform and saturated since it does not change at 400 mT [Fig. 2(f)], indicating that the superconductivity is completely broken.

Figure 3(a) shows the evolution of ZBC measured at sites apart from the vortex cores on the flat sample as marked with black triangles. Here the ZBC values are normalized by the conductance taken from the spatially averaged ZBC under 400 mT. In the plot, the normalized ZBC increases with the magnetic field linearly and then saturates. From an intersection of an upward line (the solid line) to the saturating ZBC (dashed line) [8], we found $B_{c2,\text{flat}} = 235 \pm 42$ mT, consistent with the transport measurements shown in Fig. 1(c). The GL coherence length $\xi_{\text{flat}} = 37 \pm 3$ nm at 0.36 K is then obtained using an equation

$$B_{c2,\text{flat}} = \frac{\Phi_0}{2\pi\xi_{\text{flat}}^2}, \quad (1)$$

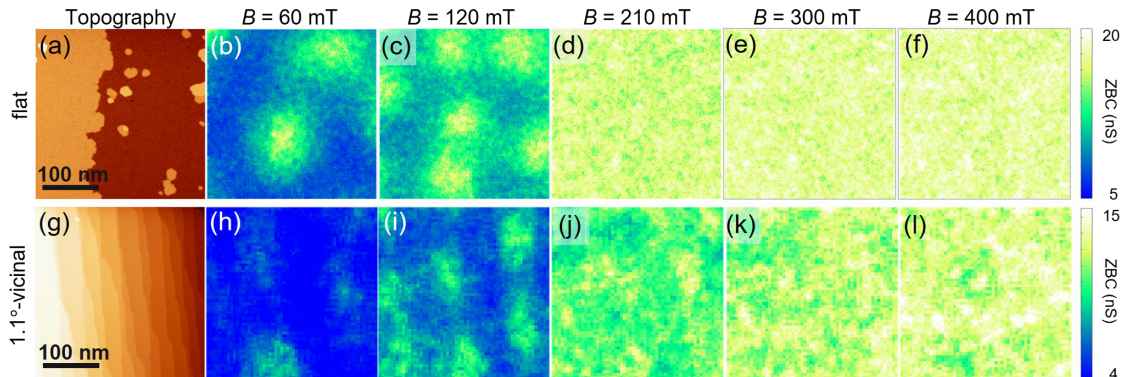


FIG. 2. (a),(g) STM images taken on (a) flat and (g) 1.1° -tilted vicinal SIC samples, respectively. (b)–(f), (h)–(l) ZBC maps under various magnetic fields taken on the same area as (a),(g), respectively. The tip height was stabilized with $V_S = 10$ mV, $I_T = 200$ pA.

where Φ_0 is magnetic flux quantum, represented as $h/2e$ using the Planck constant h and the electron charge e .

The normalization process enables us to extract features only related to the superconducting gap. On atomic layer superconductors, not only superconducting gaps but dynamical Coulomb blockade (DCB) also reduces ZBC [5,11,40–42]. Since DCB does not depend on the magnetic field, reduced ZBC observed above B_{c2} can be safely attributed to DCB. The effect of DCB can thus be eliminated by normalizing with the saturated ZBC (see more details in Sec. 9 and Fig. S7 of the Supplemental Material [25]).

We performed the same measurements on the 1.1° -tilted vicinal SIC sample. Figures 2(g)–2(l) are an STM image and corresponding ZBC maps. Under 120 mT [Fig. 2(i)], vortices are also found, but they are more or less fuzzy compared with those observed on the flat SIC, indicating phase fluctuation by the steps. Moreover, they are elongated along the step direction, and ZBC at the core of the vortices is not large compared with the saturated ZBC at 400 mT [Fig. 2(l)], which will be discussed quantitatively later. Since both are characteristic features of AJV, we tentatively attribute them to an AJV. Besides, ZBC keep increasing through 210 to 300 mT [Figs. 2(j),2(k)], which indicate that superconductivity remains above 210 mT, distinctly different from the case of the flat sample. From the ZBC evolution shown with blue squares in Fig. 3(a), we found that $B_{c2,vicinal} = 331 \pm 28$ mT, larger than $B_{c2,flat}$ and again consistent with the transport measurements. The saturated ZBC at 400 mT [Fig. 2(l)] on the tilted sample is smaller than that of the flat sample [Fig. 2(f)]. This is due to enhanced DCB by the strong localization owing to the presence of the high-density steps.

Considering Eq. (1), $B_{c2,vicinal}$ larger than $B_{c2,flat}$ may be related to reduced coherence length. The reduction in the coherence length ξ by the high-density steps is explained by the suppression of mean free path l as $\xi = \sqrt{\xi_0 l}$, where ξ_0 is the coherence length without disorder [43]. Since l in a 2D system is proportional to the conductivity, the high density steps, which work as a resistor, [4,44–48] reduce the mean free path and then coherence length in the direction perpendicular to the steps.

Since the size of the vortex is closely related to the coherence length, we focus on the size and shape of the vortices. Figure 3(b) shows cross-sectional profiles of ZBC (normalized by the respective saturated ZBCs) taken on averaged vortices shown as insets (See Sec. 10 of Supplemental Material [25]) across their centers taken on the flat sample (black triangles) and on the vicinal sample in the direction parallel ($//$, red circles) and perpendicular (\perp , blue squares) to the steps. From the profiles we found that these three profiles have a similar shape. First, on the vortices of the vicinal sample, ZBC at the center is suppressed by a factor of 0.78 ± 0.04 . Then, the suppressed profile was laterally expanded by a factor of 1.56 ± 0.27

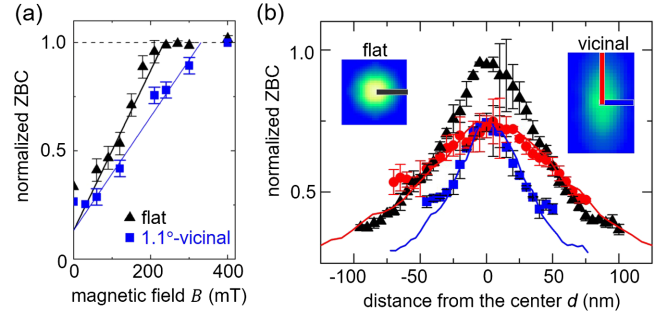


FIG. 3. (a) Evolution of ZBC as a function of the magnetic field taken on the flat (black triangle) and the vicinal (blue square) samples. The ZBC values are normalized by the spatially averaged ZBC taken under 400 mT. The solid line indicates a linear fit of ZBC before reaching the saturation and the dashed horizontal line indicates the saturated ZBC. (b) ZBC profiles across the vortex center taken on the flat substrate (black triangles) and the vicinal samples; red circles and blue squares indicate profiles taken along and perpendicular to the steps, respectively. Red (blue) lines are the profiles taken on the vortices of the flat sample multiplied by 0.78 ± 0.03 in height and by 1.56 ± 0.27 (0.76 ± 0.08) along the horizontal axis. Insets show the averaged vortices taken on the flat and vicinal samples.

and shrunk by 0.76 ± 0.08 to find good agreement with the parallel and perpendicular profiles of the vicinal sample's vortices, as shown with red and blue lines, respectively, in Fig. 3(b).

Intriguingly, the squeezing ratio in the perpendicular direction, 0.76 ± 0.08 , corresponds well to the inverse of the B_{c2} enhancement ratio ($B_{c2,flat}/B_{c2,vicinal} = 0.71 \pm 0.14$). According to the anisotropic 2D GL model [24,49–51], $B_{c2,vicinal}$ is given by

$$B_{c2,vicinal} = \frac{\Phi_0}{2\pi\xi_{\perp}\xi_{\parallel}}, \quad (2)$$

where ξ_{\perp} and ξ_{\parallel} are the coherence length along the two principal axes of anisotropy, and in the directions perpendicular and parallel to the steps in the present case. Thereby the correspondence suggests us that the B_{c2} enhancement is due to the reduced coherence length ξ_{\perp} by the presence of the steps. In order to confirm this speculation, we performed the same measurements on the SIC phase formed on a 0.5° -tilted vicinal substrate. As shown in Fig. S10 of the Supplemental Material [25], we found that B_{c2} of the 0.5° -tilted vicinal sample is 288 ± 43 mT and the squeezing ratio is 0.85 ± 0.01 , consistent with the inverse of the B_{c2} enhancement (0.82 ± 0.19). It should be noted here that we presume the coherence length along the steps are the same as that of the flat SIC phase. The elongation of the vortices along the steps is due to the formation of AJV, but the coherence length along the direction does not change since the steps do not work as disorder in the direction.

As already mentioned, the reduction in the coherence length ξ is explained by the reduced mean free path l as $\xi = \sqrt{\xi_0 l}$. According to the Drude theory, l is written as $h/e^2 k_F \rho$ in a 2D system [18], where k_F is the Fermi wave number and ρ is the resistivity. In the case of metallic monolayers formed on stepped surfaces, each step works as a resistor making the system anisotropic electrically [4,44–48]. Here, in order to model the vicinal samples electrically, we consider a 2D metallic layer with an array of parallel linear resistors at equal interval w as shown in the inset of Fig. 4(a). The normal 2D resistivity perpendicular to the steps ρ_{\perp} and parallel to the steps ρ_{\parallel} can be described [51] by

$$\rho_{\perp} = \rho_{\text{terrace}} + \rho_{\text{step}} \frac{1}{w}, \quad \rho_{\parallel} = \rho_{\text{terrace}}, \quad (3)$$

where ρ_{terrace} is the 2D resistivity on terraces, ρ_{step} is the resistivity of a single step, and w is the terrace width. Here please note that the dimensions of ρ_{terrace} and ρ_{step} are different; they are Ω and $\Omega \cdot \text{m}$, respectively. By using Eq. (3) and $l = h/e^2 k_F \rho$, we can obtain mean free path perpendicular (l_{\perp}) and parallel (l_{\parallel}) to steps, respectively.

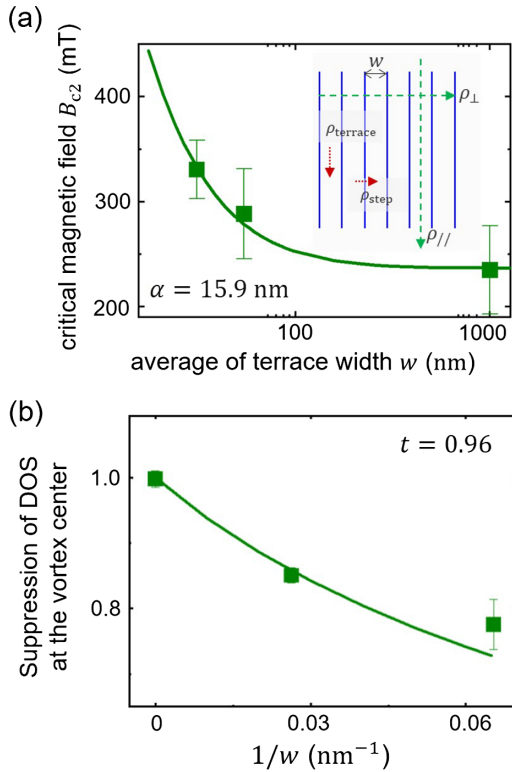


FIG. 4. (a) terrace width dependence of the critical magnetic field. The solid curve is a fitting with Eq. (5) in the main text. The inset shows a schematic of the arrayed resistors to model the vicinal SIC samples. (b) terrace width dependence of the suppressed DOS at the vortex center. The solid curve is a fitting given as $t^4 \xi_{\perp} / w$.

$$\frac{1}{l_{\perp}} = \frac{e^2 k_F}{h} \left(\rho_{\text{terrace}} + \rho_{\text{step}} \frac{1}{w} \right), \quad \frac{1}{l_{\parallel}} = \frac{e^2 k_F}{h} \rho_{\text{terrace}}. \quad (4)$$

Since the density of steps of the flat sample is sufficiently small, mean free path of the flat sample l_{flat} is equal to l_{\parallel} , leading to $\xi_{\text{flat}} = \xi_{\parallel} = \sqrt{\xi_0 l_{\parallel}}$. Then, from Eqs. (1), (2), and (4), $B_{c2,\text{vicinal}}/B_{c2,\text{flat}}$ is written as follows:

$$\frac{B_{c2,\text{vicinal}}}{B_{c2,\text{flat}}} = \frac{\xi_{\text{flat}}^2}{\xi_{\parallel} \xi_{\perp}} = \frac{\xi_{\parallel}}{\xi_{\perp}} = \sqrt{\frac{l_{\parallel}}{l_{\perp}}} = \sqrt{1 + \frac{\alpha}{w}}. \quad (5)$$

Here $\alpha \equiv \rho_{\text{step}}/\rho_{\text{terrace}}$ is a system-specific parameter with a dimension of length related to the decoupling strength. Figure 4(a) shows dependence of B_{c2} on the terrace width w estimated from the miscut angle. The data taken on 0.5° -tilted vicinal sample is also included in the plot. A solid curve is a fitted one with Eq. (5), showing good agreement when $\alpha = 15.9 \pm 1.7 \text{ nm}$. This result leads us to conclude that increasing step density effectively reduces coherence length and enhances B_{c2} . Since k_F is estimated to be $\sim 1.44 \text{ \AA}^{-1}$ in the previous report [2] and ρ_{terrace} is $\sim 550 \text{ \Omega}/\square$ from our transport measurements on the flat sample [Fig. 1(a)], we obtain $l_{\text{flat}} = h/e^2 k_F \rho_{\text{terrace}} \sim 3.3 \text{ nm}$. Using α , we can also estimate l_{\perp} as $l_{\text{flat}}(1 + \alpha/w)^{-1}$. In the case of 1.1° (0.5°) -tilted vicinal SIC samples, since $w = 15.3$ (38.0) nm, l_{\perp} is 1.6 (2.3) nm, respectively. The anisotropic ratio of resistivity $\rho_{\perp}/\rho_{\parallel} = 1 + \alpha/w$ given by Eq. (3) is estimated 2.04 ± 0.11 for the 1.1° -tilted SIC sample. This anisotropic ratio is consistent with that obtained by transport measurement performed in the van der Pauw configuration (see Sec. 12 in Supplemental Material [25]).

We then discuss the identification of AJV. One of the characteristic features of AJV is the suppression of the density of states (DOS) within the gap at the vortex core [10]. According to the calculations of AJV [10], the DOS suppression is described as t^2 , where t is the ratio of hopping strength across the step to that within the terrace. Since the width of the elongated vortex core is given by $2\xi_{\perp}$, vortices on the vicinal SIC phases cross the steps $2\xi_{\perp}/w$ times. The effective hopping strength ratio across the steps is therefore given as $t_{\perp}^{2\xi_{\perp}/w}$. Figure 4(b) shows the terrace width dependence of the suppression factor. A solid green curve is a fitting one with $t^4 \xi_{\perp} / w$, where $\xi_{\perp} = \xi_{\text{flat}}(1 + \alpha/w)^{-1/2}$ with α estimated in the B_{c2} analysis, showing a good agreement when $t = 0.96$. Considering an almost round shape of vortices trapped at a single step of the same SIC phase [12], which indicates weak decoupling, the estimated value close to 1 is reasonable. We thus conclude that the elongated vortices observed on the vicinal samples are due to the formation of AJV. They are, however, different from vortices formed on a single step that have the width of the coherence length, same as the

radius of standard round vortices, as mentioned in previous reports [10–12]. In the vicinal SIC phases, AJV are squeezed in the direction perpendicular to the steps because of the limited mean free path in the direction.

In conclusion, using both macroscopic (electrical transport) and microscopic methods we investigated superconductivity of the atomically thin Pb SIC phases formed on the vicinal Si(111) substrates. Using STM we observed elongated vortices along the steps and identified them as a squeezed AJV. Compared with AJV trapped at a single step, their width is narrowed because of the shortened coherence length due to the limited mean free path perpendicular to the steps. The reduced coherence length also explains the enhanced B_{c2} , measured in both transport and STM measurements. These observations tell us that estimating anisotropic coherence lengths from the shape of AJV and the critical field using them, which has been occasionally reported [50,52], is not appropriate. Through the investigation we found the relationship between the vortex shape and the critical field can be well controlled with the miscut angle of vicinal substrates. The monolayer superconductors formed on vicinal substrates are thus an ideal platform for the investigation of disorder-induced 2D superconductivity and its phase transition.

We thank X. Hu for fruitful discussions. This work was partially supported by Grants-in-Aid for Scientific Research (KAKENHI) from the Japan Society for the Promotion of Science (Grants No. JP18H01876, No. JP19H00859, No. JP20K15166, No. JP20K20904, No. JP21H01817, No. JP22H01961, No. JP22J13902, No. JP22K14598). Y.S. acknowledge supports by Japan Science and Technology Agency under a program called Support for Pioneering Research Initiated by the Next Generation (SPRING) (Grant No. JPMJSP 2108).

*vv22ai@issp.u-tokyo.ac.jp

†hasegawa@issp.u-tokyo.ac.jp

- [1] T. Uchihashi, *Supercond. Sci. Technol.* **30**, 013002 (2017).
- [2] C. Brun, T. Cren, and D. Roditchev, *Supercond. Sci. Technol.* **30**, 013003 (2017).
- [3] B. Sacépé, T. Dubouchet, C. Chapelier, M. Sanquer, M. Ovdia, D. Shahar, M. Feigel'Man, and L. Ioffe, *Nat. Phys.* **7**, 239 (2011).
- [4] T. Uchihashi, P. Mishra, M. Aono, and T. Nakayama, *Phys. Rev. Lett.* **107**, 207001 (2011).
- [5] Y. Noat, V. Cherkez, C. Brun, T. Cren, C. Carbillat, F. Debontridder, K. Ilin, M. Siegel, A. Semenov, H.-W. Hübers, and D. Roditchev, *Phys. Rev. B* **88**, 014503 (2013).
- [6] D. B. Haviland, Y. Liu, and A. M. Goldman, *Phys. Rev. Lett.* **62**, 2180 (1989).
- [7] I. Zaytseva, A. Abaloszew, B. C. Camargo, Y. Syryanyy, and M. Z. Cieplak, *Sci. Rep.* **10**, 1 (2020).
- [8] T. Zhang *et al.*, *Nat. Phys.* **6**, 104 (2010).
- [9] D. S. Baranov, S. Vlaic, J. Baptista, E. Cofler, V. S. Stolyarov, D. Roditchev, and S. Pons, *Nano Lett.* **22**, 652 (2022).
- [10] S. Yoshizawa, H. Kim, T. Kawakami, Y. Nagai, T. Nakayama, X. Hu, Y. Hasegawa, and T. Uchihashi, *Phys. Rev. Lett.* **113**, 247004 (2014).
- [11] F. Oguro, Y. Sato, K. Asakawa, M. Haze, and Y. Hasegawa, *Phys. Rev. B* **103**, 085416 (2021).
- [12] C. Brun *et al.*, *Nat. Phys.* **10**, 444 (2014).
- [13] K. Zhao *et al.*, *Nat. Phys.* **15**, 904 (2019).
- [14] C. Rubio-Verdú *et al.*, *Nano Lett.* **20**, 5111 (2020).
- [15] M. Liu, H. Nam, J. Kim, G. A. Fiete, and C. K. Shih, *Phys. Rev. Lett.* **127**, 127003 (2021).
- [16] R. Frindt, *Phys. Rev. Lett.* **28**, 299 (1972).
- [17] A. W. Tsien, B. Hunt, Y. D. Kim, Z. J. Yuan, S. Jia, R. J. Cava, J. Hone, P. Kim, C. R. Dean, and A. N. Pasupathy, *Nat. Phys.* **12**, 208 (2016).
- [18] Y. Saito, Y. Kasahara, J. Ye, Y. Iwasa, and T. Nojima, *Science* **350**, 409 (2015).
- [19] Y. Saito, T. Nojima, and Y. Iwasa, *Nat. Commun.* **9**, 1 (2018).
- [20] Y. Saito *et al.*, *Nat. Phys.* **12**, 144 (2016).
- [21] Y. Nakagawa, Y. Kasahara, T. Nomoto, R. Arita, T. Nojima, and Y. Iwasa, *Science* **372**, 190 (2021).
- [22] S. Ichinokura, Y. Nakata, K. Sugawara, Y. Endo, A. Takayama, T. Takahashi, and S. Hasegawa, *Phys. Rev. B* **99**, 220501(R) (2019).
- [23] H. Kim, S.-Z. Lin, M. J. Graf, Y. Miyata, Y. Nagai, T. Kato, and Y. Hasegawa, *Phys. Rev. Lett.* **117**, 116802 (2016).
- [24] A. Gurevich, *Phys. Rev. B* **46**, 3187 (1992).
- [25] See Supplemental Material at <http://link.aps.org/supplemental/10.1103/PhysRevLett.130.106002> for the sample preparation and characterization and experimental methods (Secs. 1–3) including Refs. [4] and [26–29], the analysis of results obtained by electron transport measurements (Secs. 4–7, 12) including Refs. [30,31], and the analysis of results obtained by STM (Secs. 8–11).
- [26] L. Seehofer, G. Falkenberg, D. Daboul, and R. L. Johnson, *Phys. Rev. B* **51**, 13503 (1995).
- [27] S. Stepanovsky, M. Yakes, V. Yeh, M. Hupalo, and M. Tringides, *Surf. Sci.* **600**, 1417 (2006).
- [28] C. Brand, S. Muff, M. Fanciulli, H. Pfnür, M. C. Tringides, J. H. Dil, and C. Tegenkamp, *Phys. Rev. B* **96**, 035432 (2017).
- [29] R. C. Dynes, V. Narayanamurti, and J. P. Garno, *Phys. Rev. Lett.* **41**, 1509 (1978).
- [30] H. C. Montgomery, *J. Appl. Phys.* **42**, 2971 (1971).
- [31] B. F. Logan, S. O. Rice, and R. F. Wick, *J. Appl. Phys.* **42**, 2975 (1971).
- [32] L. Aslamasov and A. Larkin, *Phys. Lett. A* **26**, 238 (1968).
- [33] K. Maki, *Prog. Theor. Phys.* **39**, 897 (1968).
- [34] R. S. Thompson, *Phys. Rev. B* **1**, 327 (1970).
- [35] Y. Imry, *Introduction to Mesoscopic Physics* (Oxford University Press, New York, 1997).
- [36] A. M. Goldman and N. Markovic, *Phys. Today* **51**, No. 11, 39 (1998).
- [37] S. Katsumoto, *J. Low Temp. Phys.* **98**, 287 (1995).
- [38] S. Ichinokura, L. V. Bondarenko, A. Y. Tupchaya, D. V. Gruznev, A. V. Zotov, A. A. Saranin, and S. Hasegawa, *2D Mater.* **4**, 025020 (2017).

- [39] N. Werthamer, E. Helfand, and P. Hohenberg, *Phys. Rev.* **147**, 295 (1966).
- [40] V. Yu. Butko, J. F. DiTusa, and P. W. Adams, *Phys. Rev. Lett.* **84**, 1543 (2000).
- [41] C. Brun, K. H. Müller, I.-Po Hong, F. Patthey, C. Flindt, and W.-D. Schneider, *Phys. Rev. Lett.* **108**, 126802 (2012).
- [42] S. Yoshizawa, H. Kim, Y. Hasegawa, and T. Uchihashi, *Phys. Rev. B* **92**, 041410(R) (2015).
- [43] M. Tinkham, *Introduction to Superconductivity*, 2nd ed. (McGraw-Hill, New York, 1996).
- [44] J. Homoth *et al.*, *Nano Lett.* **9**, 1588 (2009).
- [45] I. Matsuda, M. Ueno, T. Hirahara, R. Hobara, H. Morikawa, C. Liu, and S. Hasegawa, *Phys. Rev. Lett.* **93**, 236801 (2004).
- [46] M. Hamada and Y. Hasegawa, *Phys. Rev. B* **99**, 125402 (2019).
- [47] B. V. C. Martins, M. Smeu, L. Livadaru, H. Guo, and R. A. Wolkow, *Phys. Rev. Lett.* **112**, 246802 (2014).
- [48] S. Just, M. Blab, S. Korte, V. Cherepanov, H. Soltner, and B. Voigtländer, *Phys. Rev. Lett.* **115**, 066801 (2015).
- [49] W. E. Lawrence and S. Doniach, in *Proceedings of the 12th International Conference on Low Temperature Physics*, edited by E. Kanda (Academic Press of Japan, Kyoto, 1971), p. 361.
- [50] Q. Fan *et al.*, *Phys. Rev. B* **91**, 104506 (2015).
- [51] D.-C. Lu, Y.-Y. Lv, J. Li, B.-Y. Zhu, Q.-H. Wang, H.-B. Wang, and P.-H. Wu, *npj Quantum Mater.* **3**, 1 (2018).
- [52] A. Gyenis, B. E. Feldman, M. T. Randeria, G. A. Peterson, E. D. Bauer, P. Aynajian, and A. Yazdani *Nat. Commun.* **9**, 549 (2018).